http://journal.uir.ac.id/index.php/JGEET

E-ISSN : 2541-5794
P-ISSN : 2503-216X

Journal of Geoscience,
Engineering, Environment, and Technology
Vol 10 No 04-2/2025

RESEARCH ARTICLE

Semi-Automatic Segmentation of Igneous Rocks Thin Section Using SAGA: Application on Crystal Size Distribution (SCD) Based Residence Time Approximation

Tria Jessica Tangkulung [1], Johanes Timoty Jeremi Terok [1], Rio Priandri Nugroho [1*], Muh Nur Hidayat [1]

[1] Universitas Pertamina, Department of Geological Engineering, Jalan Teuku Nyak Arief, Jakarta, 12220, Indonesia

* Corresponding author : rio.priandri@universitaspertamina.ac.id
Received: Jul 28, 2025; Accepted: Dec 3, 2025.
DOI: 10.25299/jgeet.2025.10.1.1.24271

Abstract

Crystal Size Distribution (CSD) is a quantitative method used to assess magmatic processes such as cooling rates, crystallization durations, and crystal growth dynamics. Traditionally, mineral segmentation in CSD analysis is performed manually, which is labor-intensive, particularly for large datasets. This study investigates a semi-automatic segmentation approach to improve efficiency in analyzing thin sections of igneous rocks. The segmentation process is divided into two methods: semi-automatic segmentation using SAGA software and manual segmentation for validation. The analysis focuses on phenocrysts (>0.2 mm) and microphenocrysts (0.2–<0.02 mm), with images taken using a polarizing microscope at 4x magnification. While the semi-automatic method showed limitations due to the thin section texture and the inherent characteristics of the OBIA algorithm, it proved effective in estimating magma residence time with an average absolute error of 0.4 years. Additionally, the method demonstrated a mean regression gradient error of 79% for microphenocrysts and 55% for phenocrysts, supporting its application in magma dynamics interpretation. This approach enhances the practicality of CSD analysis, particularly in large datasets, and provides a valuable tool for studying crystallization processes in igneous rocks. However, direct application for interpreting magma dynamic should be done with caution.

Keywords: Crystal Size Distribution (CSD), Segmentation, Petrography, Residence time, Igneous rocks.

1. Introduction

Cooling history of magma can be induced from features found in igneous rocks thin sections. One of the aspects that may be revealed is residence time which can be approached by calculating the rocks' crystal size distribution (CSD) (Higgins, 2011, 2006, e.g. 2000; Higgins and Roberge, 2003; Nugroho et al., 2019; Sobolev et al., 2023; Suhendro et al., 2024; Van Der Zwan et al., 2013). This approach is traditionally conducted by delineating each crystal to be measured which may take a long time if dealing with a large dataset. In this paper, result of CSD-based residence time calculated from manual segmentation and semi-automatic segmentation using OBIA feature in SAGA (Conrad et al., 2015) is presented. This study is a development from previous study by Nugroho et al. (2024) to show how semi-automatic segmentation performs in helping to work with CSD workflow.

2. CSD Resident Time Calculation

Crystal size distribution as a workflow in geology was developed by Marsh (1998). This approach quantitatively explain magma cooling process in term of its cooling rate and residence time; time required by magma to solidify (Higgins, 2000; Marsh, 1998). The calculation of magma residence time is calculated using this formula:

$$T_r = -\frac{1}{G \times m} / 31536000 \quad (1)$$

where T_r is magma residence time (year), G is crystal growth rate (mm/year), assumed to be 10^{-8} following Marsh (1998), and m is the crystal population gradient. The constant 31,536,000 is used as a conversion factor from seconds to years.

The calculation of residence time is conducted by delineating each crystal and then calculating their size-population density. The result is then plotted into semi-log crystal size distribution graph.

3. Object-Based Image Segmentation

Object based image segmentation is a form of image classification by partitioning the images into coherent regions (Castilla and Hay, 2008) which often applied to identify geographic features as image-objects (e.g. Bechtel et al., 2008; Blaschke et al., 2014; Juniati and Arrofiqoh, 2017). Even though the initial application was to identify geographic features, few studies have shown that the algorithm can also be applied to identify geological features in hand specimen and thin section scale (Asmussen et al., 2015; Chanou et al., 2014; Nugroho et al., 2024). Nugroho et al. (2024) utilized multi input thin section images based on method developed by Asmussen et al. (2015) to segment crystals in porphyritic igneous rocks and determine the optimum threshold to be in SAGA. The multi input was applied to identify phase with internal heterogeneity and to enhance differences in hue between neighboring crystals or

phases (Asmussen et al., 2015). The relation between threshold and crystal size is expressed by this formula:

$$y = 0.0549e^{0.0245x} \quad (2)$$

where y is the average crystal size and x is the optimum segmentation bandwidth. With **Equation 2**, segmentation with the least amount of manual editing was acquired.

4. Data and Methodology

The data used in this study were 32 sets of thin section photos which were grouped based on their localities (**Table 1**). Similar to previous studies, each set of photo contains images of the rocks in plane-polarized light (PPL), cross-polarized light (XPL), plane-polarized light with gypsum (XPLG) plate, and deviating analyzer at 15°, 30°, 45°, 60°, 75°, 90° (e.g. **Fig. 1**). Each photo in 1920 x 1080 pixel in size and 571px/mm spatial resolution.

For each data set, around 30 randomly chosen crystals of each population were measured to determine the average crystal size input to be used with equation 2. Then, the calculated value for each sample was used as bandwidth input on SAGA Object-Based Image Analysis (OBIA) module. The segmented image for each data set was then manually

Table 1. Data used in this paper and their localities.

No	Population	Sample	Lithology	Type	Locality
1	A	T-01	Andesite	Intrusion	Jatiluhur intrusion complex, Purwakarta, West Jawa
2		T-02	Andesite		
3		T-03	Andesite		
4		T-04	Andesite		
5		T-05	Andesite		
6		T-06	Andesite		
7	B	T-07	Andesite	Lava	Sewu volcanic complex, Pacitan, East Java
8		T-08	Andesite		
9		T-09	Andesite		
10	C	T-10	Andesite	Lava	Sewu volcanic complex, Pacitan, East Java
11		T-11	Andesite		
12		T-12	Andesite		
13		T-13	Andesite		
14	D	T-14	Andesite	Lava	Menoreh volcanic complex, Purworejo, Central Jawa
15		T-15	Andesite		
16		T-16	Andesite		
17		T-17	Andesite		
18	E	T-18	Andesite	Lava	Menoreh volcanic complex, Purworejo, Central Jawa
19		T-19	Andesite		
20		T-20	Andesite		
21		T-21	Andesite		
22		T-23	Andesite		
23		T-24	Andesite		
24		T-25	Andesite		
25	F	T-26	Andesite	Lava	Menoreh volcanic complex, Purworejo, Central Jawa
26		T-27	Andesite		
27		T-28	Andesite		
28		T-29	Andesite		
29		T-30	Andesite		
30	G	T-31	Andesite	Lava	Mt. Muria, Central Jawa
31		T-32	Andesite		
32		T-33	Andesite		

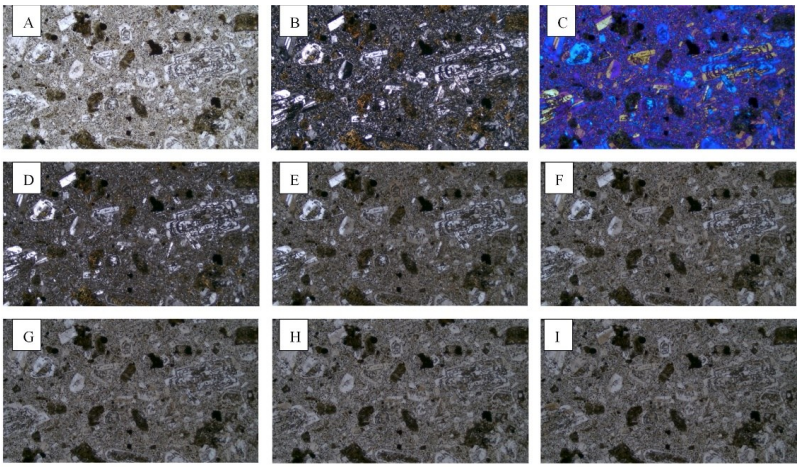

Fig. 1. Photomicrographs of thin section sample T-07: (A) Analyzer with Parallel Nicols, (B) Crossed Nicols, (C) Gypsum Plate, (D) Analyzer at 15°, (E) Analyzer at 30°, (F) Analyzer at 45°, (G) Analyzer at 60°, (H) Analyzer at 75°, (I) Analyzer at 90°.

edited to correct over- or under-segmentation (**Fig. 2**). Revised segments were measured using SAGA bounding box in convex hull tool to obtain crystal's long and short axis (**Fig. 3**). Fmin and Fmin90 obtained from the procedure were 2D aspect ratio of the crystals that only partially reflect crystals geometry. Fmin90 measurement of crystals in each data set acquired from convex hull were used as input to calculated the aspect ratio of plagioclase population in the sample using CSDSlice5 (Morgan and Jerram, 2006) resulting in the crystal population's x, y, and z axis ratio. Then, the measured Fmin90 values were put into CSD correction 1.55 (Higgins, 2000) along with calculated aspect ratio to produce CSD graph for each sample. Residence time for each sample was also calculated using **Equation 1**.

For validation, manual segmentation of each crystal was also conducted using saga polygon creation tool. The polygons were then processed similarly to the post-edited semi-automatic polygon until CSD graph and residence time were acquired. The results acquired from manual method were used to determine how effective semi-automatic segmentation is to be used in this workflow.

5. Result and Discussion

Based on the iteration for each sample, it was observed that there are differences in segmentation of crystals between semi-automatic and manual digitization (**Fig. 4**). The differences were observed on crystals with internal structures, alterations, or fractures (**Fig. 5**). It means that heterogeneity of phases within in the samples cannot be totally resolved by employing multiple input images. In addition, some small crystals of micro-phenocryst and groundmass were also mis-segmented. The issue means that object size to pixel size ratio also contributes to segmentation accuracy. Hence, minor manual editing is still necessary in the workflow (Nugroho et al., 2024).

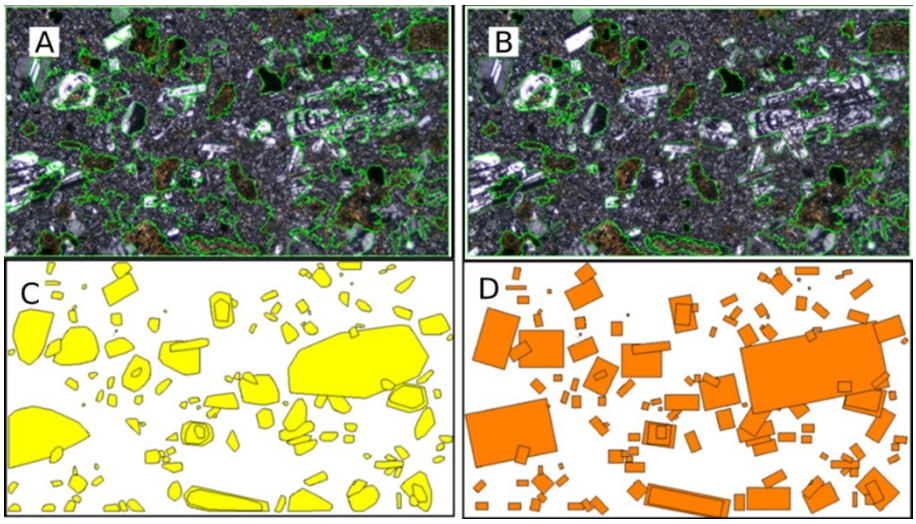

Fig. 2. An example of the semi-automatic segmentation result using the bandwidth derived from Eqn (2) is shown in (A), followed by the editing process of the segmentation output (B), the conversion of the segmented polygon into a convex hull (C), and subsequently into a bounding box (D).

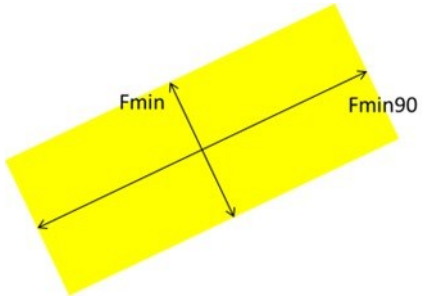

Fig. 3. Illustration of crystal size parameters extracted using Polygon Shape Indices for CSD analysis

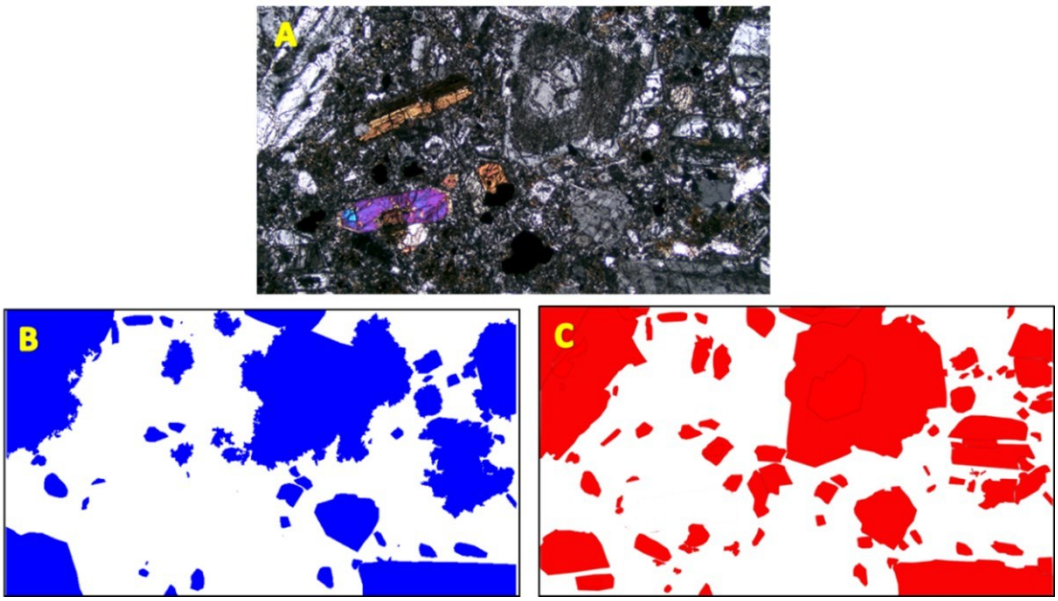

Fig. 4. (A) XPL photo from sample T-01 showing different segmentation results especially on the number of polygons of small crystals; (B) polygons from semi-automatic segmentation and (C) result from manual segmentation. Semiautomatic segmentation shows under-segmentation shown by merging of several crystals on the right of (B) and (C).

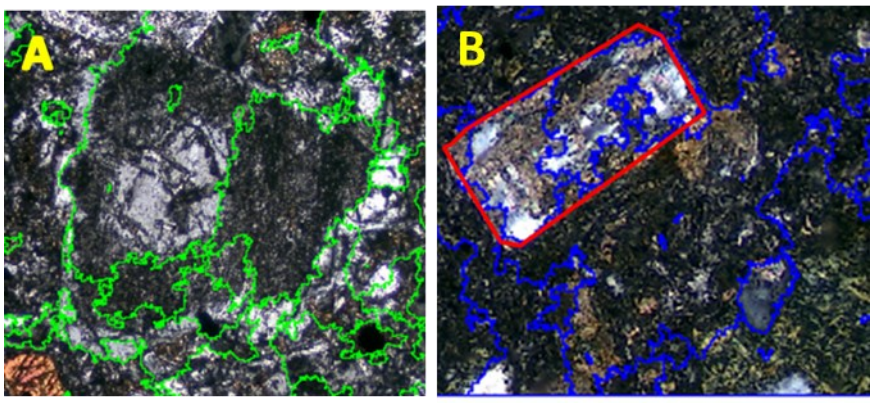

Fig. 5. (A) Internal structure in form of sieve from sample T-01; (B) alteration and fracture in sample T-19 that affected semi-automatic segmentation

Extracted polygon segment from both methods shows differences of crystals' aspect ratio, number of segments, and number of bins (**Table 2**) in the CSD calculation. This result affected the plot of CSD graph of each sample.

It can be seen that the semi-automatic segmentation produced different slopes of CSD graphs compared to the manual ones (**Table 3** and **Fig. 6**). The calculated absolute average slope deviations are 79.82% and 55.23% for micro-phenocryst and phenocryst respectively. This difference may arise from different numbers of segmented crystals and crystal population measurements which affected aspect ratio which is important in the CSD calculation. The striking different number of numbers of segment especially happens in the microphenocryst phases (**Fig. 4**). As the slope of CSD graph is one input in residence time calculations, resulted residence time acquired from semi-automatic segmentation deviates from the manual one (**Table 3**). However, in some samples, such as in T-27, both methods resulted in similar CSD (**Fig. 7**) graph and residence time (**Table 3**). Residence time calculation that resulted in negative number at sample T-14 was not included in further calculation.

Assessment of the difference of residence time shows that the deviation ranges from -1.982 to 3.592 years (**Table 3** and **Fig. 8**). The absolute average error of the semi-automatic segmentation is 0.30 for micro-phenocryst populations and 0.39 for phenocryst respectively. It shows that semi-automatic segmentation may produce acceptable residence time, especially for dealing with large datasets. However, interpretation of magma dynamics from the CSD graph should be taken with more caution as changes of regression line's gradient and y-axis interception can be interpreted as different phenomenon (e.g. **Fig. 9**).

Table 2. Tabulation of aspect ratio, number of segments, and number of bins from both methods. The x, y, and z in the table denote x, y, and z axis of measured crystal populations. Abbreviations are: M – Manual; S – Semi-automatic; mf – micro-phenocryst; f – phenocryst.

Population	No	Sampel	Aspect ratio						Number of segments		Number of bins			
			S			M			S	M	S		mf	
			x	y	z	x	y	z			mf	f	mf	f
A	1	**T-01**	1	1.15	2	1	1.05	2.05	23	90	5	4	5	4
	2	**T-02**	1	1.3	2	1	1	2.4	40	120	5	4	5	4
	3	**T-03**	1	1	1.5	1	1	1.5	32	105	5	4	5	4
	4	**T-04**	1	1	1.5	1	1.2	1.9	65	154	5	3	5	3
	5	**T-05**	1	1.15	1.7	1	1.4	2.1	76	160	5	4	5	4
	6	**T-06**	1	1.02	1.5	1	1	1.5	54	171	5	3	5	4
B	1	**T-07**	1	1.3	1.4	1	1	1.4	37	128	4	4	4	4
	2	**T-08**	1	1	1.7	1	1.25	1.8	34	128	4	4	5	4
	3	**T-09**	1	1.4	1.9	1	1.4	1.7	44	143	2	4	4	4
C	1	**T-10**	1	1	1.6	1	1.05	1.6	38	43	3	2	3	2
	2	**T-11**	1	1.7	1.8	1	1.4	1.9	12	23	4	5	4	5
	3	**T-12**	1	1.1	1.7	1	1.2	2	45	112	4	5	4	5
	4	**T-13**	1	1.05	1.15	1	1	1.15	43	114	3	4	4	4
D	1	**T-14**	1	1.5	2.8	1	1.5	3.2	38	68	5	5	5	5
	2	**T-15**	1	1.2	1.8	1	1	2.2	23	98	4	3	5	4
	3	**T-16**	1	1	1.8	1	1.5	2.2	43	55	4	5	4	5
	4	**T-17**	1	1.6	3	1	1	2.3	19	55	4	5	5	5
E	1	**T-18**	1	2	10	1	1	5	41	142	7	3	7	3
	2	**T-19**	1	1.3	1.4	1	1.3	1.4	48	156	2	2	7	3
	3	**T-20**	1	1.2	1.9	1	1	2.1	18	80	3	4	5	4
	4	**T-21**	1	1.2	1.7	1	1.2	1.5	11	36	2	3	3	3
	5	**T-23**	1	1.2	1.6	1	1.3	1.8	17	30	2	3	3	3
	6	**T-24**	1	1	1.6	1	1	2.12	16	41	2	4	5	4
	7	**T-25**	1	1.5	2	1	1.7	2	74	89	5	5	5	5
F	1	**T-26**	1	1.3	2.5	1	1.5	2.8	31	88	5	4	5	4
	2	**T-27**	1	1.4	1.5	1	2	2.4	38	67	4	4	4	4
	3	**T-28**	1	1.5	1.5	1	1.6	2	47	94	4	3	4	4
	4	**T-29**	1	1	2	1	1	1.5	16	35	5	4	5	4
	5	**T-30**	1	1.3	1.4	1	1.4	1.4	19	41	1	4	5	5
G	1	**T-31**	1	1	1	1	1	1.4	11	123	1	3	5	3
	2	**T-32**	1	1.25	2.6	1	1	2.9	18	67	5	2	5	2
	3	**T-33**	1	1.4	2.4	1	1	3.2	60	170	5	4	5	5

Table 3. Tabulation of CSD gradient and calculated residence time. Abbreviations are: M – Manual; S – Semi-automatic; mf – micro-phenocryst; f – phenocryst.

Population	Sampel	Regression gradient						Residence time						Average Absolute Error	
		M		S		Error (%)		M		S		Error			
		mf	f	mf	f	mf	f	mf	f	mf	f	mf	f	mf	f
A	T-01	-33.84	-4.06	-13.88	-3.19	-58.98	-21.58	0.09	0.78	0.23	1.00	0.13	0.21		
	T-02	-9.17	-3.85	-6.84	-6.30	-25.50	63.72	0.35	0.82	0.46	0.50	0.12	-0.32		
	T-03	-25.77	-3.89	-14.72	-3.93	-42.88	1.00	0.12	0.82	0.22	0.81	0.09	-0.01		
	T-04	-17.03	-11.53	-16.56	-6.71	-2.74	-41.81	0.19	0.28	0.19	0.47	0.01	0.20		
	T-05	-23.52	-4.25	-9.71	-7.55	-58.69	77.55	0.13	0.75	0.33	0.42	0.19	-0.33		
	T-06	-15.05	-6.57	-14.49	-13.56	-3.72	106.34	0.21	0.48	0.22	0.23	0.01	-0.25	0.09	0.22
B	T-07	-12.70	-4.72	-7.57	-5.87	-40.40	24.42	0.25	0.67	0.42	0.54	0.17	-0.13		
	T-08	-26.58	-2.02	-5.30	-2.89	-80.07	43.08	0.12	1.57	0.60	1.10	0.48	-0.47		
	T-09	14.64	-8.17	-14.83	-4.44	-201.27	-45.65	0.22	0.39	0.21	0.71	0.00	0.33	0.22	0.31
C	T-10	-2.24	-3.85	-17.57	-11.24	683.89	191.65	1.41	0.82	0.11	0.51	-1.31	-0.31		
	T-11	-12.04	3.40	-16.53	2.90	37.34	-14.71	0.26	1.08	0.19	0.92	-0.07	-0.16		
	T-12	-22.78	-6.10	-6.60	-5.00	-71.03	-18.03	0.14	0.63	0.48	0.52	0.34	-0.11		
	T-13	-16.99	-5.72	-6.85	-8.04	-59.65	40.39	0.19	0.55	0.46	0.39	0.28	-0.16	0.50	0.19
D	T-14	-23.95	-3.45	1.07	-4.28	-104.47	23.87	-2.96	0.92	0.13	0.74		0.18		
	T-15	-23.63	-4.36	-9.93	-8.68	-57.96	99.14	0.13	0.73	0.32	0.37	0.19	-0.36		
	T-16	-11.72	-4.24	-9.40	-3.48	-19.74	-17.98	0.27	0.75	0.34	0.91	0.07	0.16		
	T-17	-50.39	-1.20	-9.75	-4.74	-80.65	296.26	0.06	2.65	0.33	0.67	0.26	-1.98	0.17	0.67
E	T-18	-15.53	-4.10	-9.11	-2.60	-41.37	-36.59	0.28	0.78	0.16	1.20	-0.12	0.42		
	T-19	-9.34	-2.45	-0.75	-1.93	-91.99	-21.44	0.25	1.29	0.14	1.64	-0.11	0.35		
	T-20	-22.06	-5.30	-44.40	-2.74	101.24	-48.30	0.09	0.60	3.68	1.16	3.59	0.56		
	T-21	-11.17	-2.90	-19.31	-4.37	72.83	50.82	0.28	1.10	0.24	0.73	-0.04	-0.37		
	T-23	-12.72	-2.10	-23.10	-4.45	81.57	111.83	0.11	1.51	0.26	0.71	0.15	-0.80		
	T-24	-36.88	-3.46	-0.86	-3.05	-97.66	-11.82	0.20	0.92	0.57	1.00	0.36	0.08		
	T-25	-11.14	-4.42	-13.14	-4.27	17.94	-3.22	0.25	0.74	0.20	0.62	-0.05	-0.12	0.63	0.39
F	T-26	-28.40	-2.97	-12.04	-3.10	-57.61	4.29	0.11	1.07	0.26	1.07	0.15	0.00		
	T-27	-15.57	-3.20	-5.58	-3.30	-64.19	3.08	0.20	0.99	0.57	1.00	0.36	0.01		
	T-28	-12.53	-6.69	-15.82	-5.10	26.25	-23.80	0.25	0.47	0.20	0.62	-0.05	0.15		
	T-29	-15.79	-4.04	-22.33	-3.47	41.40	-13.91	0.20	0.79	0.14	0.91	-0.06	0.13		
	T-30	-19.64	-3.08		-1.20	-100.00	-61.02	0.16	1.03		2.64		1.61	0.16	0.38
G	T-31	-22.60	-8.82		-3.90	-100.00	-55.83	0.14	0.36		0.81		0.45		
	T-32	-11.61	-2.30	-11.73	0.78	1.02	-133.68	0.27	1.38	0.27	4.09	0.00	2.71		
	T-33	-17.93	-10.89	-12.52	-4.29	-30.20	-60.60	0.18	0.29	0.25	0.74	0.08	0.45	0.04	1.20
	Average Absolute Regression Gradient Error (%)					79.82	55.23								
	Max Manual Residence Time (positive only)					1.41	2.65	**Average error for positive error only (+)**						0.36	0.34
	Min Manual Residence Time (positive only)					0.06	0.28	**Average error for negative error only (-)**						-0.20	-0.34
	Average (absolute)					0.13	0.87	**Absolute Error**						0.30	0.39

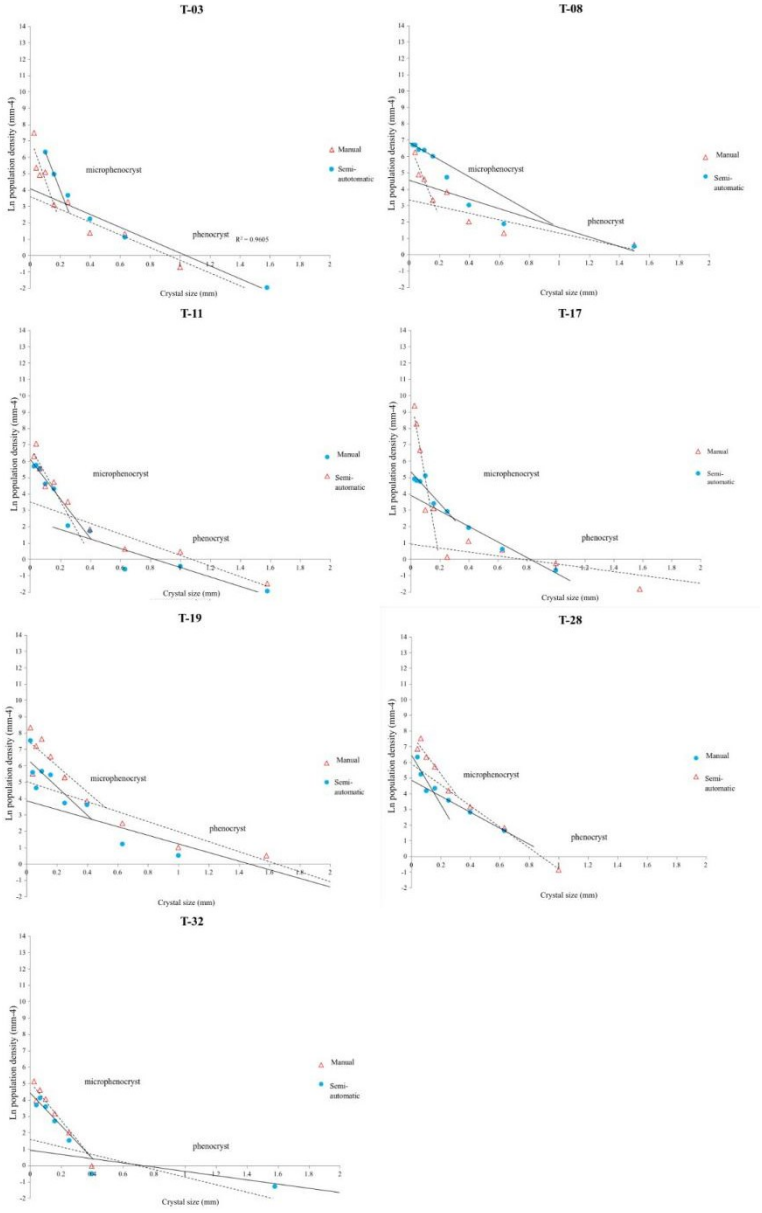

Fig. 6. Example of CSD graph of each population showing difference between semi-automatic and manual segmentation.

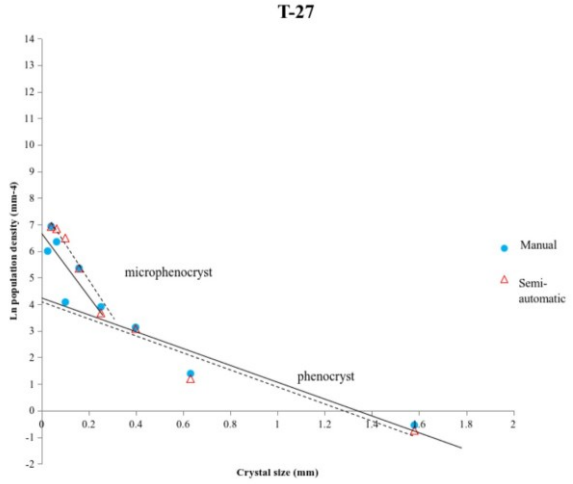

Fig. 7. CSD graph of T-27 shows similar slope calculated from both methods.

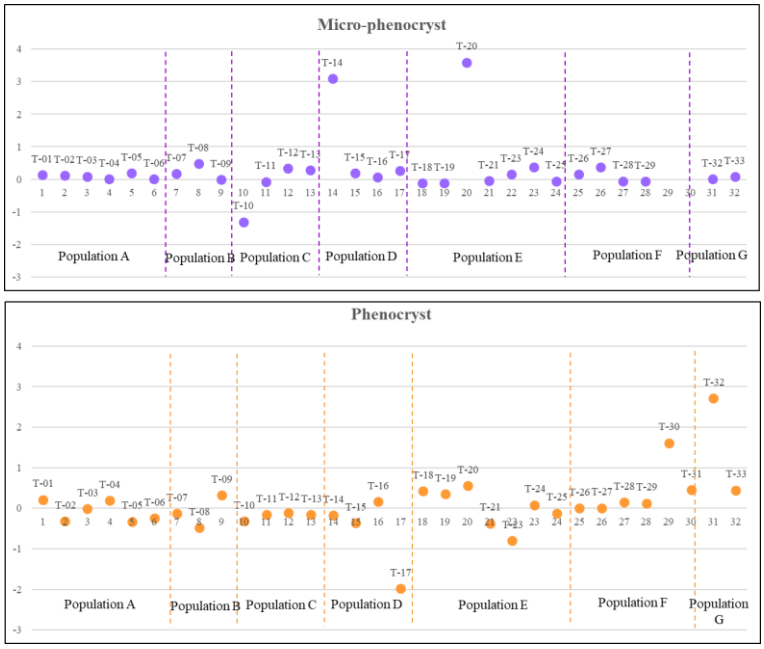

Fig. 8. Distribution residence time calculated using semi-automatic segmentation compared to the manual segmentation.

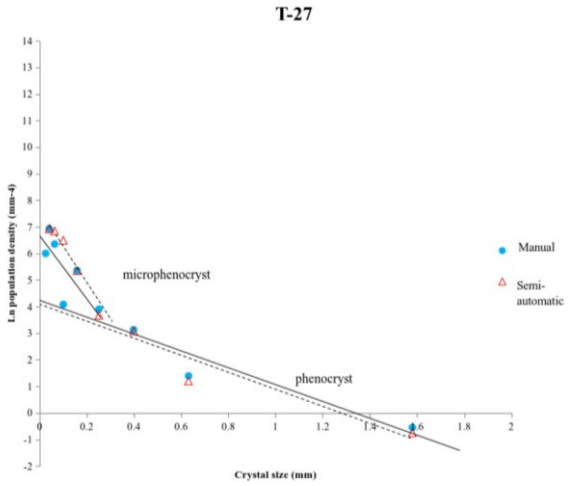

Fig. 9. Significantly different slope of T-17 that may result in different magma dynamics interpretation.

In general, mis-segmentation of the smaller-sized phase (e.g. microphenocryst) in the semi-automatic method need to be addressed. It might be solved by employing stitched images captured in higher spatial resolution. In this way, a new spatial resolution correction factor needs to be applied. In addition, more input images taken with adjusted aperture might help highlighting the phase boundaries. It should be noted that currently the semi-automatic method shows only rough CSD characteristics. Hence, manual checking and adjustment are still needed.

6. Conclusion

Semi-automatic segmentation using SAGA can be integrated into CSD workflow to determine magma residence time for a large data set with acceptable errors. However, interpretation of magma dynamics from the CSD graph should be taken with more caution and employment of higher quality input might increase the result quality.

References

Asmussen, P., Conrad, O., Günther, A., Kirsch, M., Riller, U., 2015. Semi-automatic segmentation of petrographic thin section images using a “seeded-region growing algorithm” with an application to characterize wheathered subarkose sandstone. Computers & Geosciences 83, 89–99. https://doi.org/10.1016/j.cageo.2015.05.001

Bechtel, B., Ringeler, A., Böhner, J., 2008. Segmentation for Object Extraction of Trees using MATLAB and SAGA. SAGA–Seconds Out, Hamburger Beiträge Zur Physischen Geographie Und Landschaftsökologie. Univ. Hamburg, Inst. für Geographie 1–12.

Blaschke, T., Hay, G.J., Kelly, M., Lang, S., Hofmann, P., Addink, E., Queiroz Feitosa, R., van der Meer, F., van der Werff, H., van Coillie, F., Tiede, D., 2014. Geographic Object-Based Image Analysis – Towards a new paradigm. ISPRS Journal of Photogrammetry and Remote Sensing 87, 180–191. https://doi.org/10.1016/j.isprsjprs.2013.09.014

Castilla, G., Hay, G. J., 2008. Image objects and geographic objects, in: Blaschke, T., Lang, S., Hay, Geoffrey J. (Eds.), Object-Based Image Analysis: Spatial Concepts for Knowledge-Driven Remote Sensing Applications. Springer, Berlin, Heidelberg, pp. 91–110. https://doi.org/10.1007/978-3-540-77058-9_5

Chanou, A., Osinski, G.R., Grieve, R.A.F., 2014. A methodology for the semi-automatic digital image analysis of fragmental impactites. Meteorit & Planetary Scien 49, 621–635. https://doi.org/10.1111/maps.12267

Conrad, O., Bechtel, B., Bock, M., Dietrich, H., Fischer, E., Gerlitz, L., Wehberg, J., Wichmann, V., Böhner, J., 2015. System for automated geoscientific analyses (SAGA) v. 2.1. 4. Geoscientific Model Development 8, 1991–2007.

Higgins, M.D., 2011. Textural coarsening in igneous rocks. International Geology Review 53, 354–376.

Higgins, M.D., 2006. Quantitative Textural Measurements in Igneous and Metamorphic Petrology. Cambridge University Press, Cambridge. https://doi.org/10.1017/CBO9780511535574

Higgins, M.D., 2000. Measurement of crystal size distributions. American Mineralogist 85, 1105–1116.

Higgins, M.D., Roberge, J., 2003. Crystal Size Distribution of Plagioclase and Amphibole from SoufrieÁ re Hills Volcano, Montserrat: Evidence for Dynamic Crystallization±Textural Coarsening Cycles 44, 11.

Juniati, E., Arrofiqoh, E.N., 2017. Comparison of Pixel-Based and Object-Based classification using parameters and non-parameters approach for the pattern consistency of multi scale landcover. The International Archives of the Photogrammetry, Remote Sensing and Spatial Information Sciences 42, 765–771.

Marsh, B., 1998. On the Interpretation of Crystal Size Distributions in Magmatic Systems. Journal of Petrology 39, 553–599. https://doi.org/10.1093/petrology/39.4.553

Morgan, D.J., Jerram, D.A., 2006. On estimating crystal shape for crystal size distribution analysis. Journal of Volcanology and Geothermal Research 154, 1–7. https://doi.org/10.1016/j.jvolgeores.2005.09.016

Nugroho, R.P., Disando, T., Kurniawan, I.A., Abdurrachman, M., 2019. Crystal size distribution (CSD) of plagioclase phenocryst-microphenocryst and the calculation of crystal resident times in the continuous central eruption sequences of Mount Lasem, Central Java, Indonesia. J. Phys.: Conf. Ser. 1363, 012041. https://doi.org/10.1088/1742-6596/1363/1/012041

Nugroho, R.P., Widjaya, V.V.B., Roviansah, M., 2024. Preliminary Result on Optimum Seed Generation Bandwidth for Object-Based Image Segmentation (OBIS) of Porphyritic Igneous Thin Sections. Jurnal Geologi dan Sumberdaya Mineral 25, 55–63.

Sobolev, S.N., Ariskin, A.A., Nikolaev, G.S., Pshenitsyn, I.V., 2023. Crystal Size Distribution as a Key to Understanding Protocumulus Evolution in Layered Intrusions: Experiments, Calculations, and Practice of CSD Extraction. Petrology 31, 648–663. https://doi.org/10.1134/S0869591123060097

Suhendro, I., Yuliawan, E., Zen, R.F., Rahmawati, Z.Y., Priyana, P.E., Diwijaya, S., Suhartono, M.A.T.S.P., Jonathan, A., El Zamzamy Latief, G.A., 2024. Petrology, geochemistry, and crystal size distribution of the basaltic andesite–dacite association at Mt. Sumbing, Central Java, Indonesia: Insights to magma reservoir dynamics and petrogenesis. Acta Geochim 43, 838–855. https://doi.org/10.1007/s11631-024-00673-7

Van Der Zwan, F.M., Chadwick, J.P., Troll, V.R., 2013. Textural history of recent basaltic-andesites and plutonic inclusions from Merapi volcano. Contrib Mineral Petrol 166, 43–63. https://doi.org/10.1007/s00410-013-0864-7